

PAPER • OPEN ACCESS

Numerical investigation of effects of riblets on wind turbine performance

To cite this article: J M Tubije et al 2024 J. Phys.: Conf. Ser. 2767 022023

View the article online for updates and enhancements.

You may also like

Leon Chan et al.

- Characterization of shark skin properties and biomimetic replication
 Stan R R Baeten, Ana Kochovski, Jovana Jovanova et al.
- <u>Slip length for a viscous flow over spiky</u> <u>surfaces</u> Alexei T. Skvortsov, Denis S. Grebenkov,
- Effect of structure height on the drag reduction performance using rotating disk

Musaab K Rashed, Hayder A Abdulbari, Mohamad Amran Mohd Salleh et al.



doi:10.1088/1742-6596/2767/2/022023

Numerical investigation of effects of riblets on wind turbine performance

J M Tubije, Yaqing Jin, Stefano Leonardi

Department of Mechanical Engineering, The University of Texas at Dallas, Richardson, Texas, USA

E-mail: stefano.leonardi@utdallas.edu

Abstract. In this study, systematically designed wind tunnel experiments were conducted to characterize the aerodynamic performance of a DU91-W2-250 airfoil with a riblet film. To quantify the impact of the riblet film on wind turbine performance, experimental results were used as input data for numerical simulations. Large-eddy simulations were conducted for the smooth and modified airfoils under uniform and turbulent inflow conditions. For the turbulent inflow simulations, staggered cubes were introduced upstream of the wind turbine to generate velocity fluctuations in the flow. Results from the numerical simulations show that improvements in the aerodynamic performance of the airfoil with riblets enhance the aerodynamic torque that drives the wind turbine, thereby increasing the power output. The improvement in the power coefficient with the use of the riblet film is higher for turbulent incoming wind compared to uniform flow conditions.

1. Introduction

According to the International Renewable Energy Roadmap (IRENA), to reduce CO_2 emissions by year 2050 to 9.7 Gigatonnes(Gt), high energy efficiency and increased dependence on renewable energy resources are required [1] with wind energy being 24% of the projected renewable energy source. To achieve this goal, existing and new wind turbines may be improved with devices that optimize the aerodynamic performances.

The dynamics in the near-wall region of wall-bounded flows can significantly affect the drag. Several studies show that micro-texture modifications on the surface geometry can alter the near-wall structures and can be designed to either increase mixing or reduce the drag. Riblets are microsurface protrusions aligned with the streamwise direction and spaced along the spanwise direction that can contribute to skin friction drag reduction. In the context of the transportation and logistics industry, skin friction drag contributes to around 50% of total drag [2], and riblets can be utilized to reduce fuel consumption and reduce costs. These properties of riblets have been of great interest particularly in saving millions in fuel costs in commercial transport aircrafts [3] and ships [4].

A considerable amount of research has been devoted to investigating the drag reducing mechanisms of riblets. Early studies by Walsh [5] suggest that the drag reducing effects are affected by the non dimensional riblet spacing s^+ . More recently, Garcia-Mayoral [6] proposed a new length scale which is the square of the non-dimensional groove area that collapse better with the existing experiments. These coincide with the experimental results shown by Lee [7]. Through wind tunnel experiments and a PIV setup with smoke generated from SAFEX

Content from this work may be used under the terms of the Creative Commons Attribution 4.0 licence. Any further distribution of this work must maintain attribution to the author(s) and the title of the work, journal citation and DOI.

doi:10.1088/1742-6596/2767/2/022023

and paraffin oil, Lee [7] showed that when the streamwise vortices are smaller than the riblet spacing, the riblets contribute to increase in drag as a consequence of the increased contact area. When the streamwise vortices are bigger than the riblet spacing, the vortices remain above the riblets thereby reducing the surface area exposed to the fluid carrying high speed streamwise velocity.

It has been widely shown in literature that the use of riblet films on airfoils may improve the airfoils' aerodynamic performance, albeit for particular Reynolds numbers and dimensions. Some studies delved into how this drag reducing properties of riblets can be utilized for improving the harvesting of wind energy. Sareen et al.[8] conducted experiments on a DU 96-W-180 airfoil and concluded that the drag-reducing effects of riblets on airfoils depend on size, location, angle of attack, and Reynolds number. They found that optimally placed riblets can contribute to around 4-5% drag reduction. Similarly, Chamorro et al. [9] studied the effect of riblets on an airfoil and found that depending on riblet height and geometry, riblets could provide an overall reduction in airfoil drag with up to a maximum drag reduction of 6%, but in some cases could be detrimental to the airfoil drag. Leitl [10] conducted simulations and field experiments on a AN Bonus 450/35 KW wind turbine and found that the riblets contributed to a 1.2% power increase in simulations and 13% power increase in field experiments.

However to our knowledge, there is a research gap on how a riblet film on the local blade sections affects the overall output of a wind turbine. In this paper, wind tunnel experiments were conducted to quantify the effects of the riblet film on the aerodynamic performance of a DU-91-W2-250 airfoil section. Large eddy simulations of an NREL 5MW wind turbine were carried out where the blade airfoils were replaced with DU-91-W2-250 airfoils to investigate the effects of the riblet film on the wind turbine performance.

2. Methodology

2.1. Experimental measurements

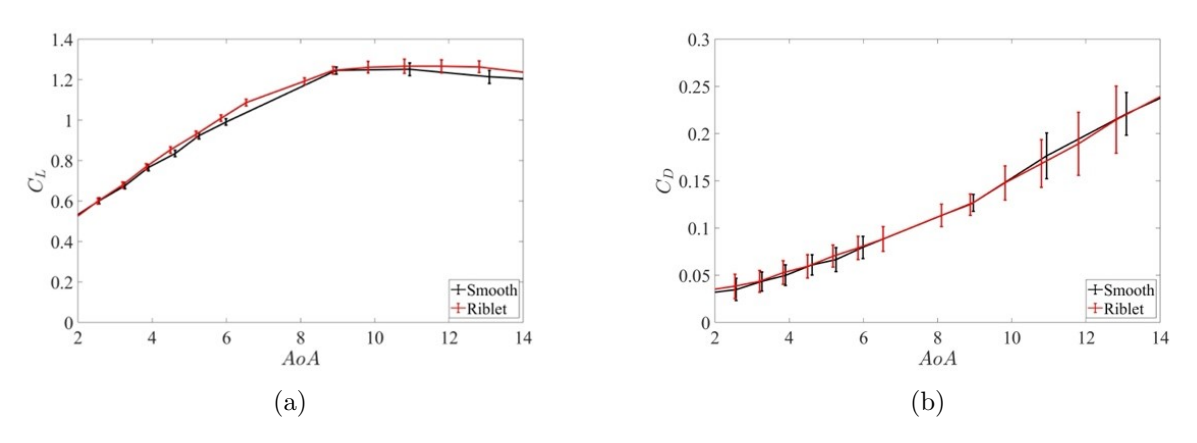


Figure 1: (a)Lift and (b)drag coefficient of DU91-W2-250 airfoil.

A DU91-W2-250 airfoil section with aspect ratio of 2 was vertically mounted on an ATI Delta sensor to measure the lift and drag loads under various angle of attacks α and chord-based Reynolds number of 650,000. The surface of the airfoil on the suction side was covered with a riblet film with pitch distance between 180 to 240 microns to evaluate its effectiveness in modulating airfoil aerodynamic performance. The riblet film extended from a location at 30% chord length from the leading edge to the trailing edge of the blade section, within which the turbulent boundary layer flow was generated on the suction side. The lift and drag coefficients were obtained via time-averaging of 60000 data points collected by the force sensor to mitigate

doi:10.1088/1742-6596/2767/2/022023

the measurement uncertainty. Measurement results highlighted that when compared to a smooth airfoil surface, the riblet film allowed to enhance the lift to drag ratio by approximately 2%, at $6 < \alpha < 8$ as shown in Fig. 1. To assess the impacts of the riblet film on the power output of a wind turbine, the experimental results were used as input for the numerical simulations.

2.2. Virtual wind turbine and numerical setup

Large Eddy Simulations (LES) were performed by solving the non-dimensional filtered incompressible Navier-Stokes equation using our in-house code. The governing equations are:

$$\frac{\partial \tilde{u}_i}{\partial x_i} = 0$$

$$\frac{\partial \tilde{u}_i}{\partial t} + \frac{\partial (\tilde{u}_i \tilde{u}_j)}{\partial x_j} = -\frac{\partial P^*}{\partial x_i} + \frac{1}{Re} \frac{\partial^2 \tilde{u}_i}{\partial x_j \partial x_j} - \frac{\tau_{ij}}{\partial x_j} + f_i^{turb}$$
(1)

where $\tilde{u_i}$ is the filtered velocity component, P^* is the filtered modified pressure, $Re = U_{ref}D/\nu$ is the Reynolds number, U_{ref} is the reference velocity, D is the diameter of the rotor, ν is the kinematic viscosity of air, τ_{ij} is the subgrid stress tensor, and f_i^{turb} is the body force term from the modelling of the wind turbine using rotating actuator disk model [11]. The filtered Navier-Stokes and continuity equations are numerically discretized in a Cartesian coordinate system using a staggered central second-order finite-difference approximation, and uses a hybrid low-storage third-order Runge-Kutta scheme to advance the equations in time. The numerical discretization is described in detail in [12].

The NREL 5 MW turbine [13] is used as a reference turbine with a rotor diameter D=126 m, and rated wind speed $U_{rated}=11.47$ m/s. The average velocity at hub height is set to $U_{hub}=0.8U_{rated}$. To investigate the effects of the riblets on the power production, the airfoil sections along the blade of the NREL 5 MW turbine were virtually retrofitted with DU-91-W2-250 airfoils while maintaining the twist along the blade length. This was done by replacing the C_L and C_D in the lookup table for the airfoils in a NREL 5 MW, with experimentally measured C_L and C_D coefficients of DU-91-W2-250 with and without the riblet film.

The computational domain is $16D \times 5D \times 10D$ in the streamwise, spanwise, and vertical directions respectively. The wind turbine is placed at 10D downstream the inlet, 2.5D in the spanwise direction. The grid is discretized into $1536 \times 768 \times 192$ points in the streamwise, spanwise, and vertical directions. The grid is stretched in the vertical direction, to allow for more grid points in the region along the diameter of the turbine blades. The spreading parameter ϵ was set as $\epsilon \geq 5\Delta x$ [14] which also satisfies Troldborg's criteria [15] $\epsilon \geq 2\Delta x$, to avoid numerical oscillations.

No slip condition is applied to the bottom boundary of the domain, to mimic the ground. Free-slip boundary conditions are applied at the top of the domain while periodic boundary conditions are applied at the boundaries along the spanwise direction. Lastly, radiative boundary conditions [16] are imposed at the outlet of the domain. The wind turbine tower and nacelle are modelled using the immersed boundary method [17], mimicking impermeability.

The inlet wind flow was generated following the power law for the atmospheric boundary layer:

$$\frac{U}{U_{hub}} = \left(\frac{y}{y_{hub}}\right)^{\beta} \tag{2}$$

where $y_{hub} = 90$ m, and the shear exponent is set to $\beta = 0.05$.

Using blade element approach, the blade is discretized into sections with local twist angles ϕ , where the lift F_L and drag F_D per unit length of the blade are locally calculated as:

doi:10.1088/1742-6596/2767/2/022023

$$F_L = \frac{1}{2}\rho U_{rel}^2 C_L(\alpha^\circ) c$$

$$F_D = \frac{1}{2}\rho U_{rel}^2 C_D(\alpha^\circ) c$$
(3)

where C_L and C_D are functions of α , ρ is fluid density, c is the section chord length, and U_{rel} is the flow velocity relative to the airfoil section given by:

$$U_{rel} = \sqrt{(U_{\theta} - \omega r)^2 + U_x^2} \tag{4}$$

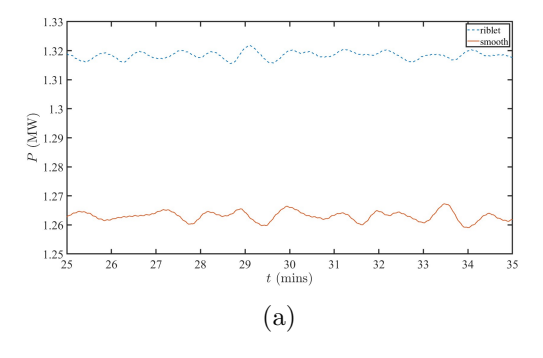
 U_{θ} is the azimuthal component of the incoming flow velocity, U_x is the streamwise component, ω is the rotor angular speed, and r the distance of the local section from the hub. For a constant U_{θ} , the ωr term contributes to an increase in U_{rel} as the section distance from hub r increases and approaches the tip of the blade. Lift and drag coefficients are interpolated from experimentally measured lift and drag curves (Fig. 1) using the local angle of attack α which is the angle between U_{rel} and the local angle of twist ϕ :

$$\alpha^{\circ} = tan^{-1} \left(\frac{U_x}{U_{\theta} - \omega r} \right) - \phi^{\circ} \tag{5}$$

The aerodynamic force F_{tan} along the blade sections are calculated by projecting the F_L and F_D into the tangential direction along the azimuthal plane:

$$F_{tan} = F_L \left(\frac{U_x}{U_{rel}} \right) + F_D \left(\frac{U_\theta - \omega r}{U_{rel}} \right) \tag{6}$$

3. Results and Discussion



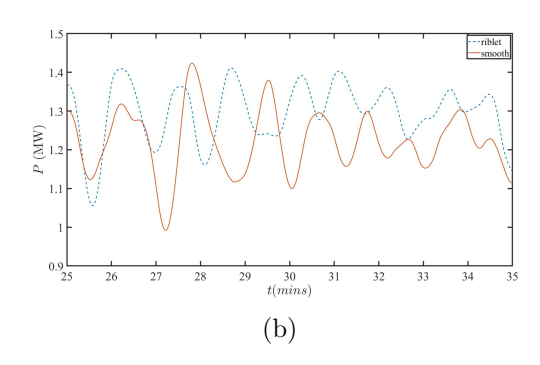


Figure 2: Power output of the wind turbine retrofitted with the DU-91-W2-250 airfoil for (a) uniform inflow, (b) turbulent inflow case.

Four test cases were conducted to investigate the effects of the riblets on the power output: uniform inflow smooth airfoil (UIS), uniform inflow riblet airfoil (UIR), turbulent inflow smooth airfoil (TIS), and turbulent inflow riblet airfoil (TIR). To generate the turbulent inflow with approximately 9% turbulence intensity one diameter upstream of the turbine, six rows of staggered 0.2D cubes were placed upstream the wind turbine, with the last row being 5.8D upstream of the rotor. In the uniform inflow cases, the power output of the UIR is always higher than UIS (Fig. 2a). For the turbulent inflow case, the behavior is more chaotic, as the instantaneous power output of TIR sometimes dips below than that of TIS albeit oscillating around a higher mean (Fig. 2b). This is because the power output is dependent on the variability in the inflow condition and the dynamics of the rotor's response to the unsteadiness and changes

in angle of attack. In both inflow conditions, riblets increase the overall power output. In the next sections, the effects of the riblets are discussed when the rotors are operating at constant angular speed and variable angular speed.

3.1. Fixed rotor speed

Two additional cases were conducted for the riblets: fixed speed uniform inflow (FUIR), and fixed speed turbulent inflow (FTIR) to investigate the effect of riblets when the turbines are operating at constant rotor angular speed equal to that of smooth airfoil turbines. In this case, torque is the only factor contributing to the change in power since ω is constant. When the riblet-film turbine is operating at the steady-state angular speed of the smooth airfoil turbines, there is a noticeable increase in the aerodynamic torque. The upward shift in lift coefficients is primarily responsible for this increase. At the same α , the values of lift coefficient C_L are higher when riblets are placed on the blade (Fig. 3). On the other hand, C_D is only partially affected by the riblets. When the riblet-film turbine is operating at the same angular speed as the smooth turbine, there is no additional contribution from U_{rel} since ω is fixed. The resulting torque and power increase is 2.86% for FUIR and 3.49% for the FTIR.

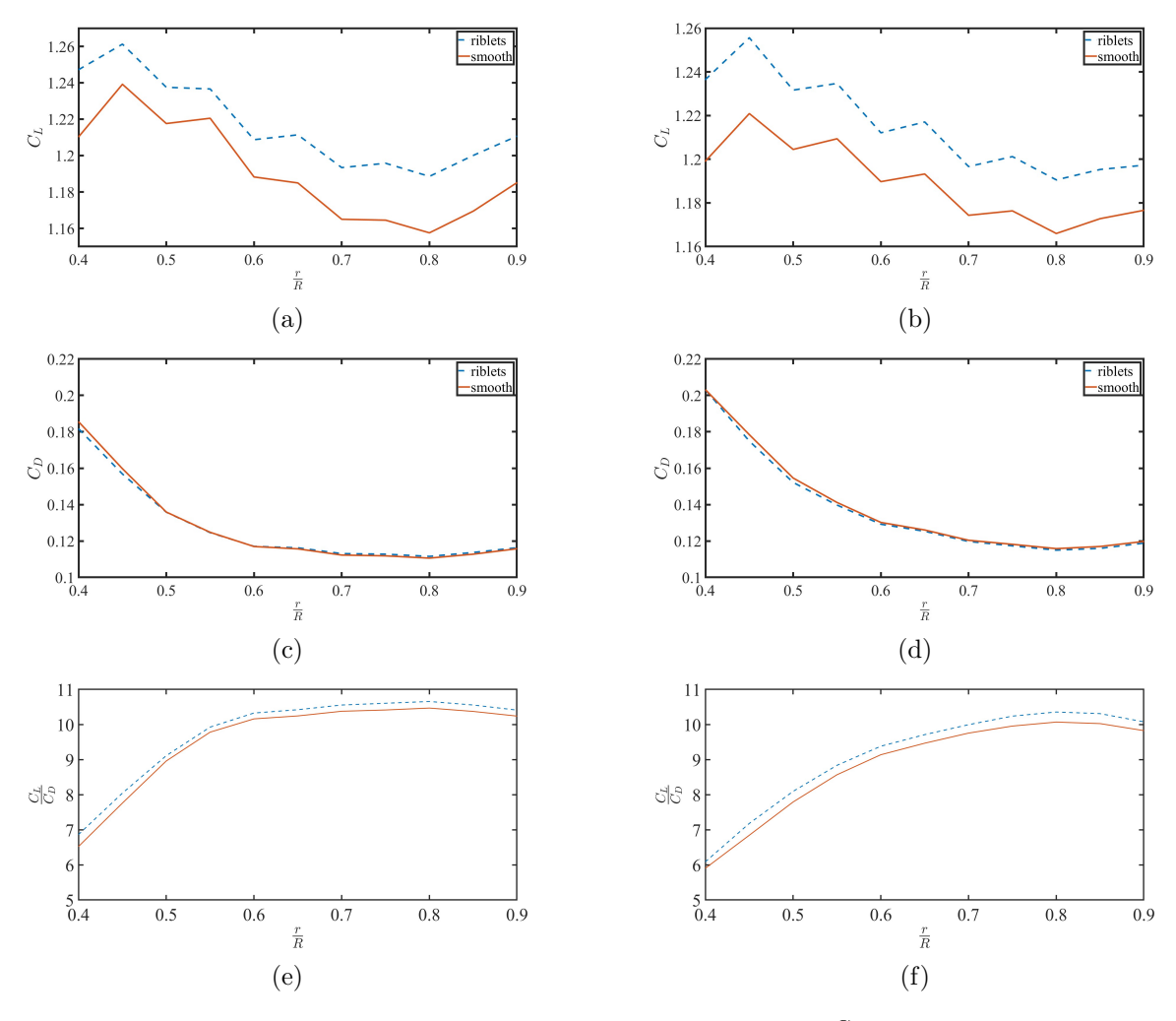


Figure 3: Time-averaged C_L , C_D , and aerodynamic efficiency $\frac{C_L}{C_D}$ along the blade sections 0.4 < r/R < 0.9 for uniform inflow case (left column) and turbulent inflow case (right column) when the riblet film case is operating at fixed rotor speed ω .

doi:10.1088/1742-6596/2767/2/022023

3.2. Variable rotor speed

In this set of simulations, the angular speed is determined through the angular momentum balance between the aerodynamic torque and the generator torque. The controller modulates the angular speed following the standard control for region 2 [18], which applies a torque gain based on the optimal tip speed ratio. When the angular speed varies, the local angle of attack and forces also change. For laminar and turbulent inflow, the airfoils with riblets exhibit an increase in both the average generator torque and average rotor speed. These improvements are due to the improved lift and drag along the length of the blade, as depicted in Fig. 4. Interestingly, these changes shift the angle of attack along the blade to lower values because of the higher tangential velocity component $(U_{\theta} - \omega r)$ in the velocity triangle. Nevertheless, it still results in an increase in T_{gen} and ω due to the larger tangential forces resulting from changes in C_L , C_D and U_{rel} .

The local angle of attack α at each section of the blade is a function of the streamwise velocity component of the wind U_x , relative tangential velocity $U_{\theta} - \omega r$, and local twist angle ϕ . At the initial stages of the simulation when steady state is not yet reached and the angular speeds of UIR and TIR are the same as the baseline (UIS and TIS respectively), the angles of attack are similar to those obtained without riblets. At this stage of the operation, C_L is significantly higher for the blades with riblets as discussed in the previous subsection. As a consequence, the tangential forces and torque are higher, leading to an angular speed which reaches a steady state higher than that relative to the smooth airfoil.

Figures 4a and 4b shows the shift in α between the cases with riblets and the cases with smooth airfoils in steady state. With the riblets, the increase in ω contributes to lower the angle of attack. Typically in the region before the stall angle, a shift to a lower α would contribute to a lower C_L . However, compared to the baseline smooth airfoil without riblets, at $9 < \alpha < 15$ the airfoils with riblets still have higher C_L and lower C_D as shown in Fig. 1 and Fig. 4. Since the rotor spins faster for the case of airfoils with riblets, U_{rel} at each local section also increases with ω as it can be inferred from equation 3.

Figure 5 shows the increase of the F_{tan} along the length of the blade with the addition of the riblet film (note that F_{tan} are the point forces from the BEM analysis of the blades). For the airfoils with riblets, three factors contribute to the increase in the F_{tan} , the combined effect of increase in C_L and decrease in C_D in some sections of the blade with riblets, particularly at 0.4 < r/R < 0.9 and the increase in relative velocity U_{rel} due to higher angular velocity ω of the rotor with the use of riblets.

For UIR, the region 0.4 < r/R < 0.6 is the one contributing the most to the increase in torque as shown in Fig. 6a. This region coincides with the highest increase in tangential forces observed in Fig. 5c, where the change is monotonically decreasing towards the blade tip. Meanwhile for TIR, the contribution of the region 0.8 < r/R < 0.9 is almost similar to 0.56 < r/R < 0.66 in Fig. 6b, despite having a smaller increase in tangential force observed in Fig. 5d. Moving towards the tip of the blade, small improvements in the tangential force become increasingly significant since the torque contribution varies linearly with the distance from the hub. The increase in the aerodynamic torque with the addition of the riblet film led to a $\Delta C_p = 4.3\%$ improvement for UIR, and $\Delta C_p = 6.6\%$ for TIR.

3.3. Loads and Torque Fluctuations

As a consequence of the riblet film improving the lift and drag coefficients, the axial forces and thrust coefficient C_t of the wind turbine also increase. Increased axial forces in the wind turbine lead to increased flapwise bending of the blades, and could potentially be detrimental to the durability of the blades. With the addition of riblets, the mean root bending moment on the blades increased by 3% for the uniform inflow and 4% for the turbulent inflow. The root-bending moment probability density function has been calculated to assess possible instantaneous high

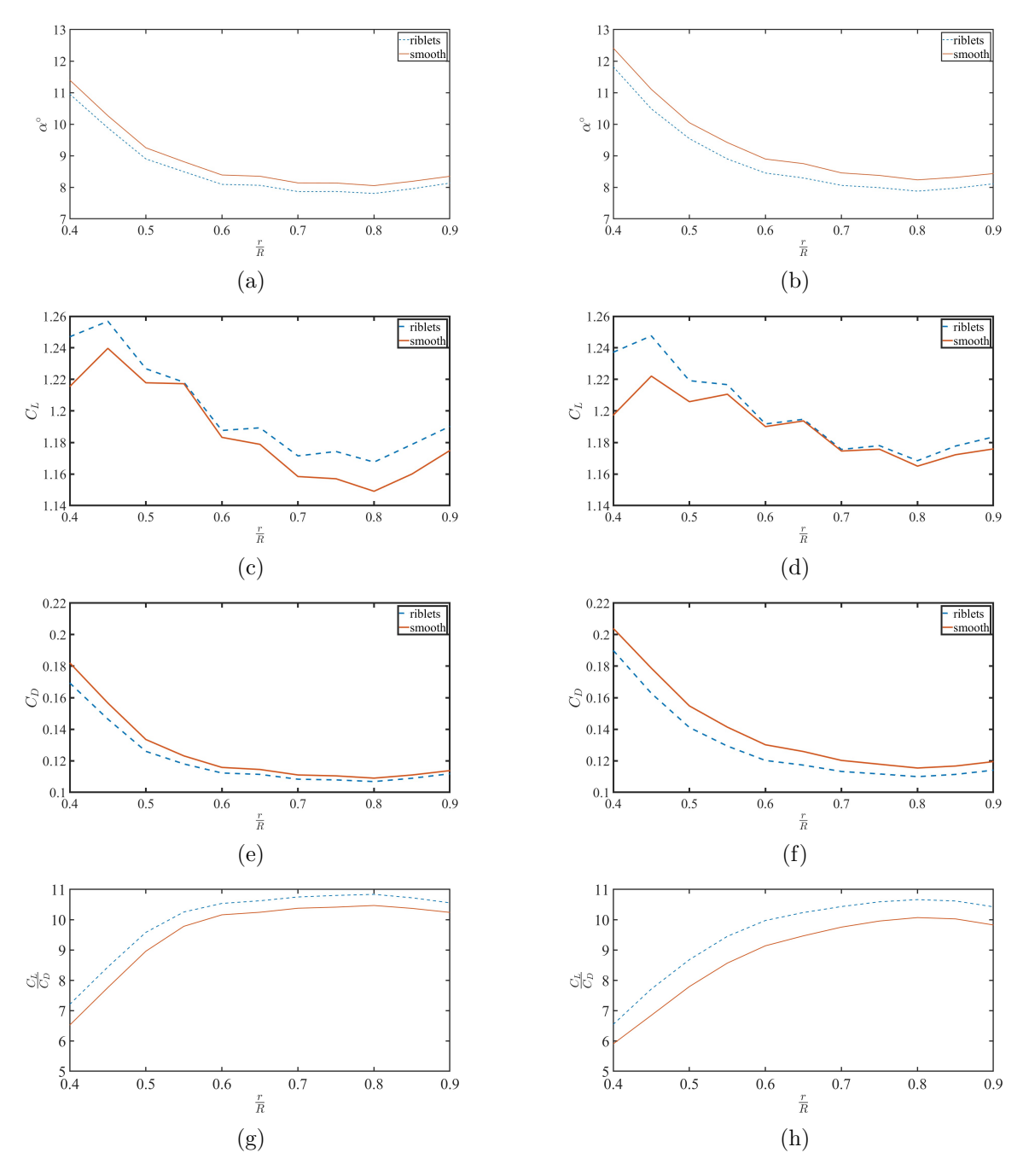


Figure 4: Time-averaged α , C_L , C_D , and aerodynamic efficiency $\frac{C_L}{C_D}$ along the blade sections 0.4 < r/R < 0.9 for uniform inflow case (left column) and turbulent inflow case (right column).

off-design loads. Figure 7 shows that, as expected, the fluctuations for the turbulent inflow is an order of magnitude higher than the fluctuations for the uniform inflow. Hence, we focused on the former. For TIR, there are comparatively more occurrences of root bending moment slightly above the mean as shown by the higher peak but the magnitude of the extreme fluctuations relative to the mean are lower. Despite that, the extreme events still have higher magnitude compared to TIS, but are closer to the mean. To better understand if these fluctuations worsen the root bending moment fatigue loads on the blade, the damage equivalent load (DEL) is

doi:10.1088/1742-6596/2767/2/022023

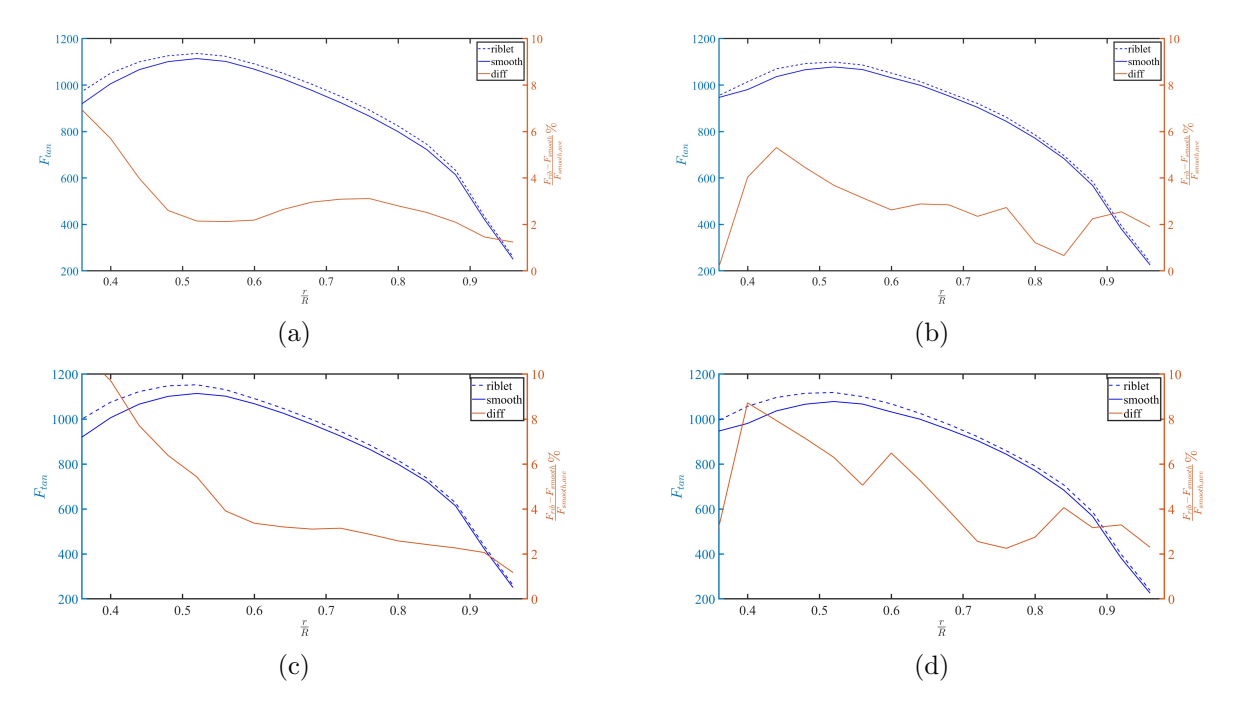


Figure 5: Resultant tangential forces $F_{tan}(N.m)$ along the blade sections 0.36 < r/R < 0.98 and the percent increase in tangential force between the airfoil with and without riblets for (a) uniform inflow fixed speed (b) turbulent inflow fixed speed (c) uniform inflow variable speed, and (d) turbulent inflow variable speed.

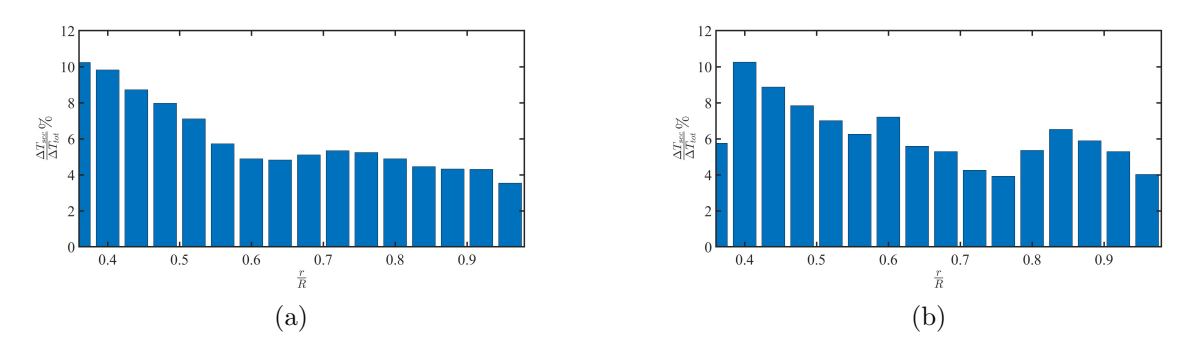


Figure 6: Percent contribution of the torque of the blade sections to the total increase in torque with the addition of riblets in the blade for (a) uniform inflow and (b) turbulent inflow.

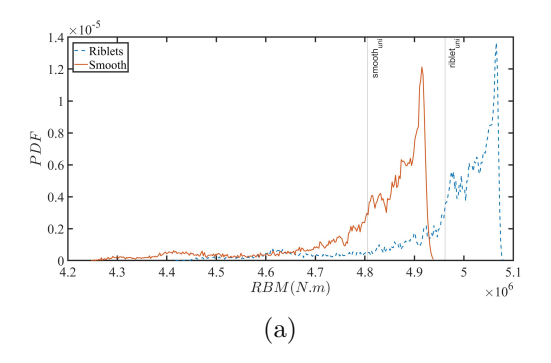
calculated and compared.

To measure the equivalent damage, the load cycles of the different root bending moments are computed using rainflow counting algorithm, then following Palgrem-Miner's rule [19], the damage equivalent load is calculated as the following:

$$DEL = \sqrt[m]{\frac{\sum\limits_{i=1}^{n} \Delta T_i^m \cdot N_i}{N_{ref}}}$$
 (7)

where m=10 is a constant based on the material's (fiberglass) Wöhler curve, ΔT_i is the load range of the i^{th} bin in rainflow counting, N_i is the number of cycles counted in the i^{th} bin, and N_{ref} is the reference number of cycles set to 1. In this particular case, $DEL_{riblet}/DEL_{smooth}$ is

doi:10.1088/1742-6596/2767/2/022023



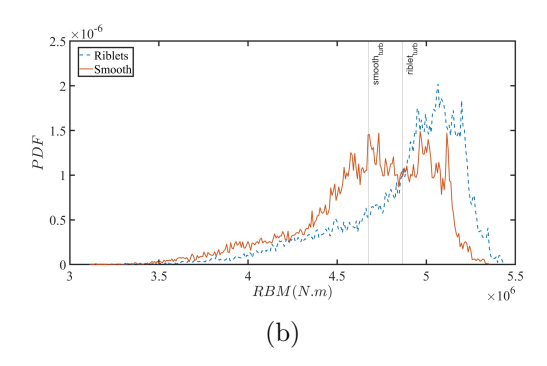
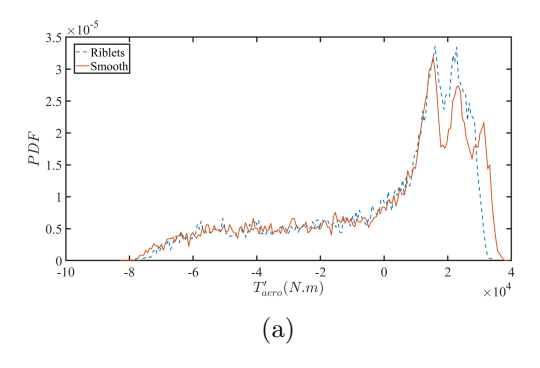


Figure 7: PDF of root bending moment for (a) uniform inflow and (b) turbulent inflow. Vertical lines represent the mean.

close to 1 implying that the addition of riblets did not have a detrimental effect on the fatigue life of the blades regarding the flapwise bending moment, despite having higher axial forces.

Torque fluctuations were also investigated, as these could cause adverse effects on the serviceable life of the gearbox due to cyclic loads. In ideal uniform-inflow winds, there are not much sources of cyclic loads aside from the interaction of the rotating wind turbine blades with the tower, and the effect of the velocity gradient in the vertical direction. However in reality, turbulent inflow is much more common and causes more fluctuations in the loads. Figure 8 shows the effect of turbulence on the aerodynamic torque fluctuations on the blade. It can be observed that the range of fluctuations for the turbulent inflow is an order of magnitude higher than that of the uniform inflow. Hence, we focused on the turbulent. With the use of the riblets, the proportion of the area under the curve above the mean is increased. This means that the riblets contribute to more incidences of positive fluctuations than negative fluctuations as compared with the smooth airfoils. With the use of riblets, the distribution of the torque fluctuations still looks similar to that of the smooth airfoils, indicating that the riblets do not modify much the torque fluctuations.



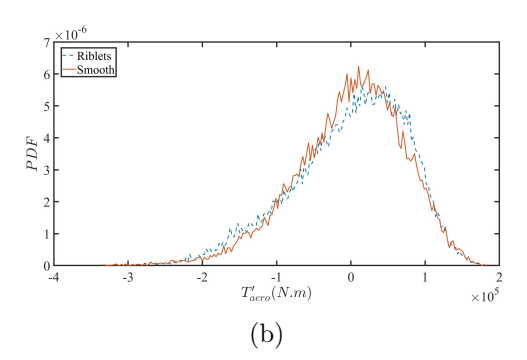


Figure 8: PDF of aerodynamic torque fluctuations for (a) uniform inflow and (b) turbulent inflow.

4. Conclusion

Wind tunnel experiments were performed to assess the efficacy of riblet films in modulating the aerodynamic characteristics of a DU91-W2-250 airfoil section. To evaluate how the riblet films affect wind turbines, LES of NREL 5MW turbine virtually retrofitted with DU91-W2-250 airfoil with and without the riblet films have been performed. When the riblet film turbines

doi:10.1088/1742-6596/2767/2/022023

are operating at the same angular speed ω of the baseline smooth case, increase in torque and power are observed due to the higher lift coefficient at same angle of attack leading to $\Delta 2.86\%$ improvement for the uniform inflow case and $\Delta 3.49\%$ for the turbulent inflow case.

Greater improvement in power generation is achieved when the riblet film turbine is controlled to work at the optimal tip-speed ratio. In this case, the angular speed increases and the angle of attack is reduced. For a uniform inflow, the use of riblets leads to 4.3% power increase. When the inflow wind is turbulent, the blades encounter a broader range of angle of attack and the riblet film contributes to a higher power increase of 6.5%. This is attributed to the riblet films delaying the critical angle of attack. Some of the angles are already in the critical stall region for the smooth airfoils but not yet for the airfoils with riblets. In this case study where only DU91-W2-250 airfoils were used in the blade, the riblets contributed to a highest increase in tangential forces in the region 0.4 < r/R < 0.6 of the blade which made that region the largest contributor in torque increase. The primary source of torque enhancement may vary when employing several combinations of airfoils and riblets as the modulation of lift and drag polars change. Moreover, the use of riblet film on the airfoil did not have a detrimental effect on the flapwise fatigue life of the blade.

Acknowledgements

This material is based upon work supported by the National Science Foundation under Award Number 1916776, Phase II IUCRC at UT Dallas: Center for Wind Energy Science, Technology and Research (WindSTAR), the WindSTAR IUCRC Members and NSF Award Number 1839733. Any opinions, findings and conclusions or recommendations expressed in this material are those of the authors and do not necessarily reflect the views of the National Science Foundation or WindSTAR members. TACC is acknowledged for providing computational time.

References

- [1] Gielen D, Boshell F, Saygin D, Bazilian M D, Wagner N and Gorini R 2019 Energy strategy reviews 24 38-50
- [2] Szodruch J 1991 Viscous drag reduction on transport aircraft p 685
- [3] Walsh M J 1990 Viscous drag reduction in boundary layers 203–261
- [4] Martin S and Bhushan B 2016 Journal of colloid and interface science 474 206–215
- [5] Walsh M and Lindemann A 1984 Optimization and application of riblets for turbulent drag reduction p 347
- [6] García-Mayoral R and Jiménez J 2011 Philosophical transactions of the Royal society A: Mathematical, physical and engineering Sciences 369 1412–1427
- [7] Lee S J and Lee S H 2001 Experiments in fluids ${\bf 30}$ 153–166
- [8] Sareen A, Deters R W, Henry S P and Selig M S 2014 Journal of Solar Energy Engineering 136 021007
- [9] Chamorro L P, Arndt R and Sotiropoulos F 2013 Renewable Energy 50 1095–1105
- [10] Leitl P A, Stenzel V, Flanschger A, Kordy H, Feichtinger C, Kowalik Y, Schreck S and Stübing D 2020 Riblet surfaces for improvement of efficiency of wind turbines p 0308
- [11] Ciri U, Petrolo G, Salvetti M V and Leonardi S 2017 Energies 10 821
- [12] Orlandi P 2000 Fluid flow phenomena: a numerical toolkit vol 55 (Springer Science & Business Media)
- [13] Jonkman J, Butterfield S, Musial W and Scott G 2009 Definition of a 5-MW reference wind turbine for offshore system development Tech. rep. National Renewable Energy Lab.(NREL), Golden, CO (United States)
- [14] Martínez-Tossas L A, Churchfield M J and Leonardi S 2015 Wind Energy 18 1047-1060
- [15] Troldborg N 2009
- [16] Orlanski I 1976 Journal of computational physics 21 251–269
- [17] Orlandi P and Leonardi S 2006 Journal of Turbulence N73
- [18] Johnson K E, Pao L Y, Balas M J and Fingersh L J 2006 IEEE Control Systems Magazine 26 70–81
- $[19] \ \ Cosack \ N\ 2010 \ \textit{Fatigue load monitoring with standard wind turbine signals}\ \ Ph.D.\ thesis\ Universit\"{a}t\ Stuttgart$